Spatial correlations of spontaneously down-converted photon pairs detected with a single-photon-sensitive CCD camera

**Bradley M. Jost, Alexander V. Sergienko,
Ayman F. Abouraddy, Bahaa E. A. Saleh,
and Malvin C. Teich**

*Quantum Imaging Laboratory, Department of Electrical and Computer
Engineering, Boston University, Boston, MA 02215*

bjost@bu.edu, teich@bu.edu
http://ece.bu.edu/ECE/faculty/homepages/teich/qil/QImaging.html

Abstract: A single-photon-sensitive intensified charge-coupled-device (ICCD) camera has been used to simultaneously detect, over a broad area, degenerate and nondegenerate photon pairs generated by the quantum-optical process of spontaneous parametric down-conversion. We have developed a new method for determining the quantum fourth-order correlations in spatially extended detection systems such as this one. Our technique reveals the expected phase-matching-induced spatial correlations in a 2-f Fourier-transform system.

References

1. D. C. Burnham and D. L. Weinberg, "Observation of simultaneity in parametric production of optical photon pairs," *Phys. Rev. Lett.* **25,** 84–87 (1970).
2. D. N. Klyshko, "Transverse photon bunching and two-photon processes in the field of parametrically scattered light," *Zh. Eksp. Teor. Phys.* **83,** 1313–1323 (1982) [*Sov. Phys. JETP* **56,** 753–758 (1982)].
3. A. Joobeur, B. E. A. Saleh, and M. C. Teich, "Spatiotemporal coherence properties of entangled light beams generated by parametric down-conversion," *Phys. Rev. A* **50,** 3349–3361 (1994).
4. A. Joobeur, B. E. A. Saleh, T. S. Larchuk, and M. C. Teich, "Coherence properties of entangled light beams generated by parametric down-conversion: Theory and experiment," *Phys. Rev. A* **53,** 4360–4371 (1996).
5. M. H. Rubin, "Transverse correlation in optical spontaneous parametric down-conversion," *Phys. Rev. A* **54,** 5349–5360 (1996).
6. P. H. Souto Ribeiro, "Partial coherence with twin photons," *Phys. Rev. A* **56,** 4111–4117 (1997).
7. B. E. A. Saleh, A. Joobeur, and M. C. Teich, "Spatial effects in two- and four-beam interference of partially entangled biphotons," *Phys. Rev. A* **57,** 3991–4003 (1998).
8. J. Peřina, Z. Hradil, and B. Jurčo, *Quantum Optics and Fundamentals of Physics* (Kluwer, Boston, 1994).
9. L. Mandel and E. Wolf, *Optical Coherence and Quantum Optics* (Cambridge, New York, 1995), Ch. 22.
10. A. A. Malygin, A. N. Penin, and A. V. Sergienko, "Spatiotemporal grouping of photons in spontaneous parametric scattering of light," *Dokl. Akad. Nauk SSSR* **281,** 308–313 (1985) [*Sov. Phys. Dokl.* **30,** 227–229 (1985)].
11. B. E. A. Saleh and M. C. Teich, *Fundamentals of Photonics* (Wiley, New York, 1991), Ch. 16.
12. *Princeton Instruments Catalog of High Performance Digital CCD Cameras: September, 1995,* Princeton Instruments, Inc., Trenton, NJ 08619; we used a slow scan model ICCD-576-G/RB-E detector with a third-generation intensifier for all experiments.
13. B. E. A. Saleh and M. C. Teich, *Fundamentals of Photonics* (Wiley, New York, 1991), Ch. 4.

14. A. Gatti, L. A. Lugiato, G.-L. Oppo, R. Martin, P. Di Trapani, and A. Berzanskis, "From quantum to classical images," *Opt. Express* **1,** 21–30 (1997). http://epubs.osa.org/oearchive/source/1968.htm
15. D. N. Klyshko, *Photons and Nonlinear Optics* (Gordon and Breach, New York, 1988), Ch. 6.
16. A. V. Belinskii and D. N. Klyshko, "Two-photon optics: diffraction, holography, and transformation of two-dimensional signals," *Zh. Eksp. Teor. Fiz.* **105,** 487–493 (1994) [*JETP* **78,** 259–262 (1994)].
17. D. V. Strekalov, A. V. Sergienko, D. N. Klyshko, and Y. H. Shih, "Observation of two-photon 'ghost' interference and diffraction," *Phys. Rev. Lett.* **74,** 3600–3603 (1995).
18. T. B. Pittman, Y. H. Shih, D. V. Strekalov, and A. Sergienko, "Optical imaging by means of two-photon quantum entanglement," *Phys. Rev. A* **52,** R3429–R3432 (1995).
19. T. B. Pittman, A. V. Sergienko, D. V. Strekalov, Y. H. Shih, M. H. Rubin and D. N. Klyshko, "Two-photon geometric optics," *Phys. Rev. A* **53,** 2804–2815 (1996).
20. P. H. Souto Ribeiro and G. A. Barbosa, "Direct and ghost interference in double-slit experiments with coincidence measurements," *Phys. Rev. A* **54,** 3489–3492 (1996).
21. B. E. A. Saleh, S. Popescu, and M. C. Teich, "Generalized entangled-photon imaging," in *Proceedings of the IEEE LEOS 1996 Annual Meeting* (Boston, MA, 1996), pp. 362–363.
22. E. Jakeman and J. G. Rarity, "The use of pair production processes to reduce quantum noise in transmission measurements," *Opt. Commun.* **59,** 219–223 (1986).

1. Introduction

Photon pairs generated by the nonlinear quantum-optical process of spontaneous parametric down-conversion (SPDC) [1] exhibit remarkable time and space correlations. The wavelengths and emission angles of the pairs, and hence the photon correlations, are governed by the interaction geometry and the phase-matching conditions within the nonlinear material via conservation of energy and momentum. The consequent quantum fourth-order temporal- and spatial-coherence properties of these twin beams are most simply characterized by an entanglement time T_e and an entanglement area A_e (or equivalent polar- and azimuthal-entanglement angles)[2-7]. The entanglement time of the pairs has been determined using a variety of interferometric techniques [8, 9].

The spatial correlations were first observed using photomultiplier tubes behind pinholes that selected conjugate pair locations in a down-converted beam [10]. More recently, using a pair of discrete detectors, the entanglement angles of degenerate photon pairs were measured [4]. This paper reports a measurement of the overall spatial pair correlations using an intensified charge-coupled-device (ICCD) camera that simultaneously detects degenerate and nondegenerate photons from the down-converted beam over the broad area of the CCD array. Our results can be viewed as the spatial analog of the timing coincidence measurements that are found in the SPDC literature.

2. Experiments

We used an ICCD camera, which is similar to that shown in Fig. 1, as the photon-detection device throughout our experiments. It has as its first surface a photocathode from which an incident photon induces the ejection of an an electron; such electrons can be produced over the entire surface of the photocathode. The electrons are ejected into a microchannel-plate electron-multiplier stage where they are amplified in number. The resulting electron bunches impinge upon a phosphor screen that emits photons in response, thus providing intensification of the incident light distribution [11]. These photons are transmitted into a fiber-optic bundle that is attached to the CCD-array input. Hence, each incident photon makes many photons available for detection by the CCD array. Of course, the process is not ideal—the quantum efficiency (electrons/photon) of the photocathode of our ICCD camera is $\eta \sim 25\%$ [12]. Further specifications of the ICCD camera are as follows: the array size is 576 x 384 pixels (12.7 x 8.5 mm; each pixel is $22 \times 22 \ \mu\text{m}^2$), the dynamic range is 16 bits/pixel, the dark current at -45°C is <

16 electrons/(pixel s) (we operated our ICCD at -35°C), and the amplifier gain allows sensitivities to 100 counts (analog-to-digital units or digitized bits) per photoelectron.

Figure 1.   The main components of an ICCD camera showing the photocathode front surface, microchannel-plate amplifier, fiber bundle, and CCD wafer package [12].

Down-converted light was generated by propagating an unpolarized multimode 40-mW He–Cd laser pump beam with a wavelength of 325 nm through a nonlinear SPDC crystal. As shown in the basic setup illustrated in Fig. 2, the laser beam was first directed through a prism to separate undesired plasma tube emissions at other wavelengths, which were blocked with an iris. A 650 ± 35 nm bandpass filter was used to reduce the irradiance of the residual pump light that remained mixed with the down-converted light and, after passing through a lens, the output photons were detected with the ICCD camera. The intensifier gain was set to its maximum value. Two different type-I (extraordinary-polarized pump, ordinary-polarized signal and idler) nonlinear down-conversion crystals were used in our experiments as described below.
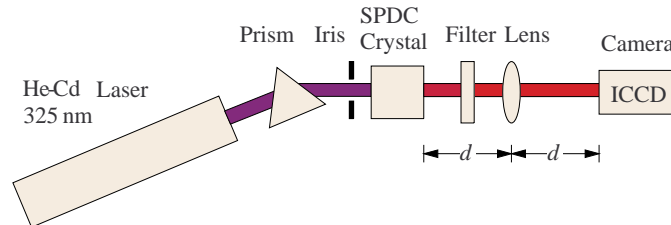

Figure 2.   Illustration of the basic spontaneous parametric down-conversion optical system.

We investigated two simple geometries. The first was a one-to-one 4-f imaging system (Fig. 2 with $d = 2f$) in which a 50-mm diameter lens with focal length $f = 75$ mm was used. Ideally, for a very thin crystal, even though they are emitted in different directions the down-converted signal and idler pair will appear at the same point at the surface of the ICCD since they are emitted from the same point within the crystal. For a thick crystal, the limited depth of field of the imaging system will lead to a range of pair separations at the ICCD surface. We used a $15 \times 15 \times 25$ mm^3 LiIO$_3$ crystal (cut angles $\theta_c \approx 59°$ and $\phi_c \approx 45°$) tilted $\approx 1°$ relative to the optic axis for noncollinear degenerate down-conversion in this experiment. An example of an image from this system is shown in Fig. 3(a). The region of larger spot density relative to that of the rest of the picture comprises the imaged down-converted light emitted from the crystal. It is difficult in this case to separate the residual pump photons from the down-converted photons. Autocorrelation analyses of such images did not provide useful results, possibly because of the spatial overlap of the undesired residual pump light with the desired down-converted light and because the thick crystal produced too wide a range of photon-pair separations.
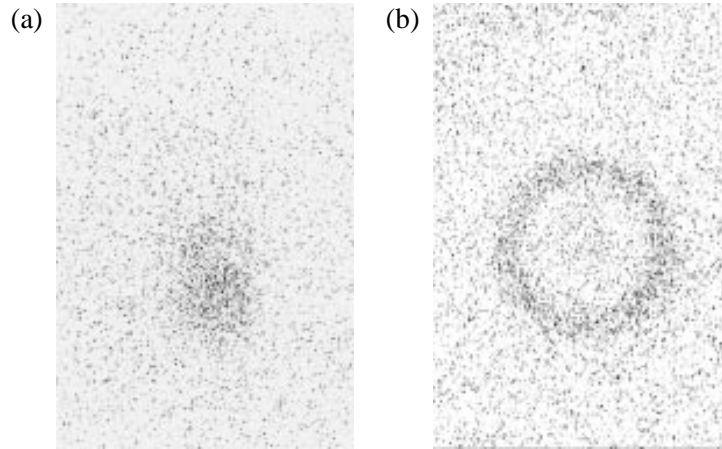
Figure 3.   Contrast-adjusted negative pictures obtained from (a) a 4-f one-to-one imaging system (4-μs exposure time) and (b) a 2-f angle-to-position optical system (100-μs exposure time). In addition to the features sought, there is a spatially random background-noise distribution.

The second geometry was a 2-f system (Fig. 2 with $d = f$) in which the front surface of the ICCD was placed in the focal plane of the lens. A standard photographic 50-mm $f/1.4$ lens focused to infinity was used. Here, the lens performs a spatial Fourier transform [13] and each angle of the down-converted light is mapped onto a circle at a particular radius from the optic axis. Since the SPDC phase-matching conditions lead to angles that differ in accordance with the wavelengths of the photons, an annulus of down-converted light is formed. Pictures of the down-converted light were obtained using a $6 \times 6 \times 1$ mm^3 BBO crystal (cut angles $\theta_c \approx 36.2°$ and $\phi_c \approx 90°$) tilted $\approx 1°$ relative to the optic axis to obtain noncollinear degenerate down-conversion. The tilt was adjusted so that the annulus of down-converted light filled an appropriate region of the ICCD array [see Fig. 3(b)]. Although our ICCD camera is not designed to determine the wavelengths of the detected photons, wavelength information is embedded in pictures taken with this configuration. In these experiments the configuration was modified to further reduce the residual pump light: a pair of Glan-Thompson analyzers (one to polarize the pump beam prior to the crystal and the other, which was rotated ninety degrees relative to the first, to reduce the pump light after the crystal) was used along with a high-reflectivity mirror at 325 nm that was placed after the second analyzer. Note that the residual pump light lies at radii smaller than those within the annular region of interest. A detailed analysis of this case is described in the next section.

A pair of pictures that appears similar to that shown in Fig. 3 was recently obtained in an investigation of SPDC classical spatial-irradiance patterns (Fig. 5 in Ref. [14]). Those pictures, however, comprise classical (relatively high irradiance) measurements of only the signal beam. In distinction, our pictures contain combined signal and idler detections as pairs of correlated single-photon events.

3.   Analysis

Our goal is to experimentally determine the form of the fourth-order spatial correlation (photon coincidence) of the down-converted light. That is, we desire to determine the uncertainties of the radius δr and angle $\delta \phi$ from ideal, as shown in Fig. 4. The SPDC photon-emission wavelengths and angles are determined by the phase-matching conditions: $\omega_p = \omega_s + \omega_i$ and $\mathbf{k}_p = \mathbf{k}_s + \mathbf{k}_i$ where the pump, signal, and idler frequencies and wavevectors are ω_p, ω_s, ω_i and $\mathbf{k}_p$, $\mathbf{k}_s$, $\mathbf{k}_i$, respectively. In the ideal case of an infinitely

extended crystal and pump beam, each down-converted photon has a partner whose emission angle can be exactly determined.
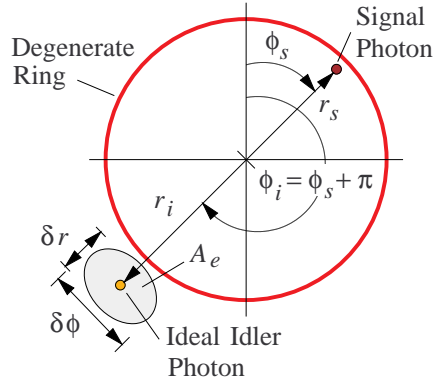

Figure 4. Illustration of the spatial relationship between the signal and idler photons in a 2-f angle-to-position optical system. The signal and idler photon-detection points are specified by their radii $r_{s,i}$ and angles $\phi_{s,i}$. In practice, an area of locations A_e is possible for the idler because of uncertainty in the radius δr and the angle $\delta\phi$.
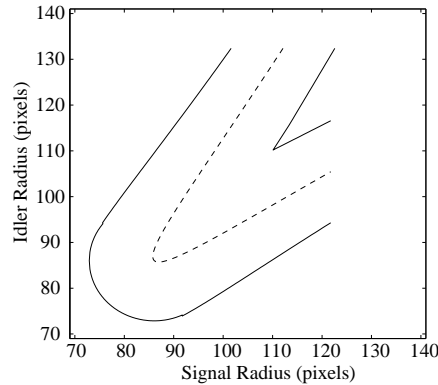

Figure 5. Theoretical continuous-plane-wave pump phase-matching as a function of signal and idler radii (in ICCD camera pixels measured from the center of the rings) for a BBO crystal with cut angles $\theta_c = 36.2°$, $\phi_c = 90°$; tilted 1° with respect to the optic axis; and with a 325-nm pump wavelength. Results are shown for ideally pumped down-conversion to wavelengths in the range 600-700 nm for an infinitely long crystal (dashed curve) and for a 1-mm long crystal (solid curves defining a boundary within which pairs can be phase-matched).

In a system comprising finite crystals and beams, the correspondence between the signal- and idler-photon spatial locations is blurred because there are uncertainties in the energies and the transverse and longitudinal wavevectors [3-7](see Fig. 5, for example). The principal origins of the spread in the spatial- and temporal-correlation functions are the finite crystal size, both transversely (when the crystal cross-section is smaller than that of the pump beam) and longitudinally, and the transverse structure of the pump beam. A less important contribution arises from the finite pump bandwidth. Yet another consideration is diffraction in the optical system. All of these factors contribute to the uncertainty in the location of the idler photon over a region defined as the entanglement area A_e, as shown in Fig. 4. In Fig. 5, we provide the theoretically expected ideal phase-matching curve (dashed) as well as the spread in possible values of the radii that arises from the longitudinal wavevector uncertainty associated with a finite crystal length l_c: $\delta r_{s,i} \propto 1/[k_p l_c \sin(ar_{s,i})]$ where a is a proportionality constant

associated with the SPDC photon-emission angles [15].

In our efforts to develop a feasible correlation analysis technique involving the 2-f configuration, we first considered an idealized situation in which a signal photon occurring at angle ϕ_s and radius r_s is matched by one and only one idler photon at $\phi_i = \phi_s + \pi$ and r_i (see Fig. 4). In the degenerate case, the signal and idler wavelengths are equal and $r_i = r_s$. Suppose we observe the down-converted light with a noiseless CCD camera that detects each incident photon such that a single corresponding infinitesimal pixel is excited. If we had full knowledge of the remainder of the optical system, and if we were able to perfectly isolate the down-converted light from the residual pump light, we could use the phase-matching conditions to determine the exact position and wavelength of each idler photon that is associated with each detected (signal) photon. The correlation analysis of experimentally obtained data is straightforward in this case: one need simply compare each pixel with its diametrically opposed pixel along with its neighbors. However, this simple procedure cannot be gainfully deployed in non-ideal systems.

In practice, the arrivals of the photons are detected by intercepting the down-converted rings with an ICCD camera that amplifies the individual photons in such a way that each incident photon typically excites a small patch of pixels with various levels of illumination. Moreover, minor distortions of the rings are introduced by the optical system and the spatial discretization of the microchannel-plate amplifier, the fiber-optic coupler, and the CCD array. We initially attempted to use the idealized correlation analysis described above but failed to produce meaningful results primarily because of two practical difficulties: the center of the down-converted photon annulus is difficult to precisely identify (and is not very useful for full-ring analysis if the rings are distorted), and errors are introduced by the registration (mapping) of the rings in translating from a rectilinear (pixel) to a polar coordinate system. These problems introduce uncertainties into the analysis and degrade our ability to observe the correlations. Consequently, we devised a technique that provides a more robust measure of the correlation by limiting our angular ranges to small diametrically opposed sectors and comparing small patches instead of single pixels within these sectors.
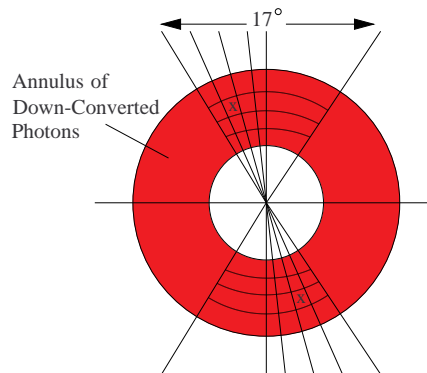

Figure 6.   Illustration of the mapping and correlation analysis scheme with the 2-f optical system. A pair of x's mark examples of diametrically opposed patches with the same radii.

Our correlation analysis scheme is illustrated in Fig. 6. We first determined the center of the annulus of the down-converted light (within $\approx \pm 2$ pixels), which defines the center of a polar coordinate system. We then chose a 17° sector and labeled it the signal sector. The intersection of the sector with the down-conversion annulus defined an annular segment. This was subdivided into seventeen subsegments 1° wide; each of these was further subdivided into patches three pixels thick along the radial direction.

Thus, we obtained a set of concentric annular regions each of which contained seventeen patches.

The radius and polar angle identified each such patch. All of the values of the rectilinear pixels in each patch were summed to provide a set of numbers within our polar coordinate system. A radius-dependent threshold, the level of which was empirically determined by incremental adjustment and testing with the images, was implemented at this stage to reduce both background noise and effects due to the patch-size dependence on radius.

The cross-correlation was obtained by comparing the numbers associated with the set of seventeen signal-polar patches lying at a given radius with those associated with an equal number of idler-polar patches (obtained in the same manner) located at an arbitrary radius but at a complementary angle (the annular regions comprising the sets of seventeen patches are therefore opposite one another). This was repeated for annular regions that were symmetrically distributed about the horizontal and vertical axes, and at $\pm 45°$ to them. Results from each of the four analyses were normalized to their own maximum and then averaged to produce a plot that displays the *radial* dependence of the correlation function. The correlations between non-diametrically opposed segments were subsequently calculated to determine the *angular* dependence of the correlation function. Standard correlation measurements were used.
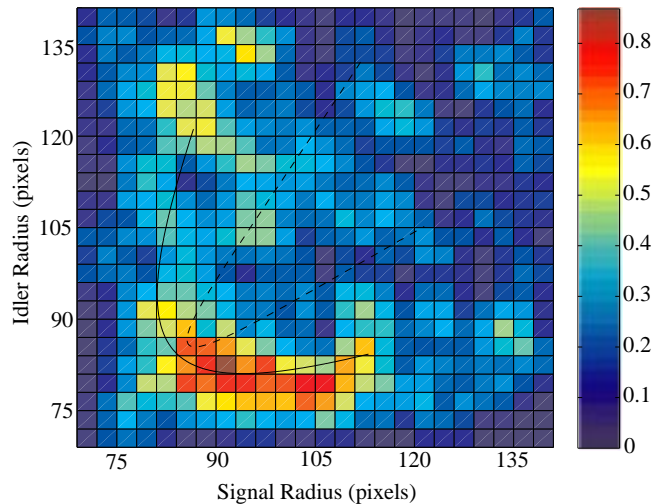

Figure 7. Experimental spatial correlation (color plot) as a function of the signal and idler radii (1 pixel corresponds to an angular spread $\approx 0.021°$ in the radial direction) obtained from an analysis of 150 images taken with a 2-f system. The radii begin at slightly less than the minimum detected down-conversion radius and extend slightly beyond the maximum detected down-conversion radius as they appear in Fig. 3(b). Two ideal theoretical phase-matching curves for type-I BBO with a cut angle $\phi_c = 90°$ and a 325-nm pump beam incident on the crystal at an angle of $1°$ are provided: the $\theta_c = 36.2°$ result as in Fig. 5 (dashed curve) and a fit with $\theta_c = 36.7°$ and a $-2°$ shift in the down-conversion angles (solid curve).

The result that obtains from an analysis of 150 2-f-system pictures taken with the BBO crystal and a 100-μs exposure time (we estimate that each such picture contains ~ 10–100 matched photon-pair detections) is shown in Fig. 7. The average correlation as a function of the signal and idler radii is shown in false color. The correlations in this figure were calculated as described above for each picture, the 150 results were averaged, and each data point was further averaged over its nearest neighbor's values to smooth the results. The measured correlation function forms a "V"-like region tilted

45° with respect to vertical. The correlations are relative values; thus, for example, a signal–idler radii pair with correlation equal to 0.8 is eight times more likely to have matched illumination in the corresponding patches than a pair with correlation equal to 0.1. Points along the diagonal that extends from the origin correspond to the degenerate case.

In Fig. 7 we have also plotted curves corresponding to the theoretically expected locations of high correlation obtained under ideal SPDC phase-matching conditions. Two plots are provided. The first (dashed curve) is the plot from Fig. 5 which was obtained using an estimate of the crystal parameters and the geometry of our experimental configuration. The second (solid curve) is a fitted curve in which the crystal-cut angle and the deviation of the down-conversion detection angle from ideal provide two adjustable parameters. Our experimentally obtained regions of high correlation lie within the vicinity of both theoretical curves. We note that the parameters of the fitted curve, which provides a better match, might be obtained from more accurate evaluations of the refractive indices of the down-conversion crystal and the crystal cut. The measurement is generally well matched with both theoretical results yet we anticipate that further refinements in our experimental measurement and analysis techniques will provide even better correspondence.

It is of interest to compare our results with those obtained using a pair of discrete detectors in a prior investigation [4]. Our measured width at degeneracy (along the diagonal) is $\delta r \approx 6$ pixels which corresponds to 0.126° (2.2 mrad). To measure how the correlations were affected when the diametric opposition requirement was relaxed, we repeated the analysis using incremental 1° steps around 180°. We found that there is a very rapid dimunition of the high correlation regions. From our analysis, we determined that $\delta\phi < 1°$ (17 mrad). The values of $\delta\phi$ and δr obtained here are several times larger than those obtained in the earlier investigation [4], most likely because we used a crystal with one-tenth the length and configured for one-tenth the degenerate photon-emission angle.

4. Discussion

We have described a method by means of which the quantum spatial-pairing correlations of both degenerate- and nondegenerate-SPDC photons can be measured over a broad spatial area using a single-photon-sensitive ICCD camera. This research is supportive of the development of entangled-photon imaging systems [16-21]. Such systems provide some interesting capabilities. For example, the paired nature of the entangled photons means that if one photon is detected, there is also a partner photon at a corresponding position and time. Suppose one member of each pair is used to illuminate an object and the other member of each pair is simply detected. Knowledge of such a detection informs us that there should also be a photon that either passed through or was scattered by the object. This information can be used along with coincidence detection to significantly reduce background, detector, and quantum noise in the image, relative to conventional techniques, potentially to sub-shot-noise levels [22]. Furthermore, the signal and idler paths are functionally equivalent in terms of their optical properties [16, 21]. Consequently, non-absorptive optical elements can be moved from the signal path to the idler path and *vice versa,* without affecting the overall imaging properties of the system. ICCD cameras are therefore viable compact alternatives to scanned small-area detectors in such experimental configurations.